Calculation of the Infrared Intensity of Crystalline Systems. A Comparison of Three Strategies Based on Berry Phase, Wannier Function, and Coupled-Perturbed Kohn–Sham Methods

Calculation of the Infrared Intensity of Crystalline Systems. A Comparison of Three Strategies Based on Berry Phase, Wannier Function and Coupled-Perturbed Kohn-Sham Methods.

R. Dovesi,[*,†] B. Kirtman,[‡] L. Maschio,[*,†] J. Maul,[†] F. Pascale,[¶] and M. Rérat[§]

†*Dipartimento di Chimica, Università di Torino and NIS -Nanostructured Interfaces and Surfaces - Centre of Excellence, http://www.nis.unito.it, Via P. Giuria 5, 10125 Torino, Italy*

‡*Department of Chemistry and Biochemistry, University of California, Santa Barbara, California 93106, United States*

¶*Laboratoire de Physique et Chimie Théoriques, UMR 7019, Université de Lorraine, CNRS, 54506 Vandœuvre-lès-Nancy, France*

§*IPREM UMR5254, Université de Pau et des Pays de l'Adour, 64000 Pau, France*

E-mail: roberto.dovesi@unito.it; lorenzo.maschio@unito.it

Abstract

Three alternative strategies for the calculation of the IR intensity of crystalline systems, as determined by Born charges, have been implemented in the CRYSTAL code, using a gaussian type basis set. One uses the Berry Phase (BP) algorithm to compute the dipole moment; another does so, instead, through well localized crystalline orbitals (Wannier Functions, WF); and the third is based on a Coupled Perturbed Hartree-Fock or Kohn-Sham procedure (CP). In WF and BP the derivative of the dipole moment with respect to the atomic coordinates is evaluated numerically, whereas in CP it is analytical. In the three cases very different numerical schemes are utilized, so that the equivalence of the obtained IR intensities is not ensured a priori, but rather is the result of the high numerical accuracy of the many computational steps involved. The main aspects of the three schemes are shortly recalled, and the dependence of the results on the computational parameters (number of k points in reciprocal space, tolerances for the truncation of the Coulomb and exchange series, and so on) is documented. It is shown that in standard computational conditions the three schemes produce IR intensities that differ by less than 1%; this difference can be reduced by an order of magnitude by acting on the parameters that control the accuracy of the calculation. A large unit cell system (80 atoms per cell) is used to document the relative cost of the three schemes. Within the current implementation the BP strategy, despite its semi-numerical nature, is the most efficient choice. That is because it is the oldest implementation, and is based on the simplest of the three algorithms. Thus, parallelism and other schemes for improving efficiency have, so far, been implemented to a lesser degree in the other two cases.

Introduction

The theoretical prediction of the vibrational spectrum is an extremely useful tool for the characterization of crystalline solids in general, and in particular when materials are difficult

to analyze experimentally as is the case of point defects, or when the system is affected by low crystallinity. Moreover, when accurate experimental data are at hand, ab initio quantum mechanical simulations can be used as a complementary source of information (*e.g.* in detecting silent or low-intensity modes). If, besides the wavenumbers, the IR intensities are also available, the complete spectrum can be generated.

As a matter of fact, both the accurate measurement and the simulation of the infrared spectrum of a solid are considerably more challenging than for molecules in the gas phase. The practical applicability of such a synergistic approach between theory and experiment, as described above, has become possible only in recent years and has had an important impact on many fields such as earth sciences,[1] heterogeneous catalysis,[2] supramolecular chemistry[3] and terahertz spectroscopy.[4]

The IR intensity of a mode is proportional to the square of the unit cell dipole moment derivative with respect to the normal coordinate describing the mode. Evaluation of the dipole moment is trivial for finite systems (molecules, or polymers and slabs along non periodic directions), but requires special attention and tools in periodic directions, since it is an ill-defined quantity[5,6] when evaluated as the mean value of the **r** operator with respect to the crystalline orbitals (CO), which are usually represented in a basis of Bloch functions. This problem can be by-passed in different ways:

1. By using the Berry phase (BP) theory, due to King-Smith and Vanderbilt,[7] and Resta[6] (see also Ref. 5), that permits one to evaluate the dipole moment difference between two geometries. This scheme was implemented in the CRYSTAL code by Dall'Olio et al in 1997 for the calculation of the spontaneous polarization (ferroelectricity). It was extended later on to piezoelectricity[8,9] and, finally, to the IR intensity in CRYSTAL09 by Claudio Zicovich-Wilson. In the case of IR intensities the following procedure is employed. The Hessian for obtaining the vibrational frequencies is evaluated numerically by displacing each atom a small amount along the three Cartesian coordinates and, then, computing the difference between the analytical gradients at the displaced

and equilibrium geometries. In parallel, the Berry phase difference is evaluated for each displacement. The IR intensity is, then, obtained from the Berry phase difference between the 3N (N is the number of atoms) displaced geometries and the equilibrium one. A numerical derivative with respect to the reciprocal space lattice vector **k** is also involved, which makes the accuracy of the method dependent on the chosen sampling of reciprocal space.

2. Through the localized Wannier Function (WF) scheme implemented a number of years ago (2001) by Claudio Zicovich and some of the present authors[10,11] which was used, at first, for an easy and intuitive description of the electronic structure of crystalline compounds in terms of chemical concepts, such as lone pairs, shared electrons, and covalent vs. ionic bonds.[12] It was subsequently employed for the calculation of the spontaneous polarization of ferroelectric materials and the piezoelectric tensor,[9,13] and then, more recently, for the calculation of the IR intensity of crystalline systems.[14] The latter is obtained as the difference between the sum of the reference WF centroids at two geometries. In the present case, the difference involves the equilibrium geometry and each one of the distorted geometries used in the numerical derivative scheme, in exactly the same way as for the BP method.

   Wannier functions are also one of the key ingredients for the Local MP2[15–17] approach to post-Hartree-Fock correlation energy in crystalline compounds.

3. By using the Coupled Perturbed Hartree-Fock (CPHF) scheme of Dupuis et al.[18,19], as adapted for electric fields in periodic systems[20–22] and implemented in the CRYSTAL code by Ferrero et al.[23,24], who included coupled perturbed Kohn Sham (CPKS) as well. In combination with the standard analytical treatment of geometric energy gradients, based on the orbital energy weighted density matrix, this yields the desired second derivatives of the energy with respect to the field and atomic displacements.[25,26]

The three schemes are quite different.

The first scheme, BP, operates on the crystalline-orbital eigenvectors in reciprocal space, and is performed separately for the equilibrium and displaced geometries. It is a calculation that requires the full overlap matrix between the occupied Crystalline Orbitals (CO) at each **k** point with its three neighbors, and scales quadratically with the basis set size (since the number of occupied CO is proportional to the basis set size).

The WF scheme, based on a Boys-like localization, operates mostly in direct space and requires a Self-Consistent procedure.[10] However, the complete localization scheme is applied only for the equilibrium geometry. The WFs of the distorted structures are obtained by projecting the WFs of the undistorted structure onto the corresponding occupied manifolds. Owing to the small geometry differences between the equilibrium and displaced points (0.01 Å for an individual atomic coordinate), and taking into account that only the centroids (first order moment) of the WF are required, the projection technique yields WFs that are sufficiently localized for the accurate computation of the dipole moment derivative.

The third algorithm, CPHF/CPKS, is completely analytical and all calculations are performed at the equilibrium geometry. The first-order perturbation equations must be solved self-consistently in reciprocal space for each Cartesian component of the electric dipole moment.

The aim of the present paper is to compare these three alternative strategies with respect to their relative merits and limitations. These formalisms, which have been presented in detail previously, will be reviewed here and, then, critically analyzed and compared.

Our paper is organized as follows: first, the general scheme adopted for the calculation of the vibrational frequencies is summarized. Then the role of the derivatives of the dipole moment with respect to the atomic positions (also known as Born charges), Z, in the calculation of the IR intensities, is briefly recalled. The following sections summarize the main equations used for the calculation of Z with a Gaussian type basis set in the three alternative methods: the Berry phase treatment; the path that uses Wannier functions; and the strategy

based on the CPHF-KS scheme. The last two sections are devoted to the presentation of results for two systems, α-quartz and pyrope, followed by some discussion and conclusions. Most of the formal development for the three schemes appears in the Supplementary Material section. Equations in the Supplementary Material are labelled as S.X, where X stands for the eq. number.

Methods

Dynamical matrix

The Dynamical Matrix (DM)

For symmetry reasons, only the DM of the Central Zone Point (Γ point, or $\mathbf{k} = \mathbf{0}$) of the Brillouin zone is required for obtaining the IR (as well as Raman) spectra. The analytical part of the DM is given by

$$W_{\alpha i,\beta j}(\mathbf{k} = \mathbf{0}) = \frac{1}{\sqrt{M_\alpha M_\beta}} H_{\alpha i,\beta j} \tag{1}$$

where H is the Hessian matrix, $M_{\alpha(\beta)}$ is the mass of atom $\alpha(\beta)$ and i, j are atomic Cartesian coordinates. The square root of the eigenvalues of W are the TO (transverse Optical) vibrational frequencies, whereas the eigenvectors determine the vibrational normal modes (see www.crystal.unito.it/prtfreq/jmol.html for graphical animation of the modes) used to obtain the mode intensities (see eq. 4-9 below).

First derivatives of the total energy E with respect to atomic displacements, $\upsilon_{\alpha j} = \partial E/\partial u_{\alpha j}$, are calculated analytically ($u_{\alpha j}$ is the displacement coordinate with respect to equilibrium), whereas second derivatives at $u_{\alpha j} = 0$ are calculated numerically either as:

$$H_{\alpha i,\beta j} \approx \frac{\upsilon_{\alpha i}(0, \cdots, u_{\beta j}, \cdots) - \upsilon_{\alpha i}(0, \cdots, 0, \cdots)}{u_{\beta j}} \tag{2}$$

or by averaging over equal positive and negative displacements:

$$H_{\alpha i,\beta j} \approx \frac{v_{\alpha i}(0,\cdots,u_{\beta j},\cdots) - v_{\alpha i}(0,\cdots,-u_{\beta j},\cdots)}{2u_{\beta j}} \quad . \tag{3}$$

In our calculations the displacements $u_{\beta i}$ are set equal to 0.01 Å.

The Born charges and related quantities

The α-atomic Born tensor is the key quantity for the calculation of IR intensities. This tensor is defined as follows:

$$Z^*_{\alpha,ij} = \frac{\partial}{\partial u_{\alpha j}}\Big(\frac{\partial E}{\partial \mathcal{E}_i}\Big) \equiv \frac{\partial}{\partial u_{\alpha j}}\mu_i \tag{4}$$

in which $\mathcal{E}_i$ is the i-th component of an applied electric field and μ is the cell dipole moment.

It is well known[5,6] that, in crystalline systems, μ depends upon the arbitrary choice of the unit cell. On the contrary, the dipole moment difference between two geometries of the same system (i.e. the polarization per unit cell) is well-defined. Consequently, the partial derivatives in eq. 4 can be estimated numerically (for the BP and WF strategies) from the differences generated by small atomic displacements as in the calculation of the energy second derivatives (see eq. 2 or 3). The formula for Born charges per unit volume (V) then reads:

$$Z^*_{\alpha,ij}/V = \Delta P^{\alpha,ij}_{el} + \Delta P^{\alpha,ij}_{nuc} \tag{5}$$

The nuclear contribution is easily evaluated as

$$Z^{*\,(nuc)}_{\alpha,ij} = \zeta_\alpha \delta_{ij} \tag{6}$$

where ζ_α is the atomic number of nucleus α.

The IR intensity

We seek the Born charge tensor in the basis of vibrational modes. The matrix of eigenvectors t of the mass-weighted Hessian W transforms the Cartesian atomic displacements $\mathbf{u}_{\alpha j}$ into normal coordinates, $\mathbf{Q}_p$, through a suitable mass-weighting factor:

$$\mathbf{Q}_p = \sum_{\alpha i} \left(t_{\alpha i,p} \sqrt{M_\alpha} \right) \mathbf{u}_{\alpha i} \tag{7}$$

Then the Born charges, in terms of normal coordinates, become:

$$\bar{Z}_{p,i} = \sum_{\alpha j} t_{\alpha j,p} Z^*_{\alpha,ij} / \sqrt{M_\alpha}. \tag{8}$$

The intensity of the p-th IR mode is proportional to the square of the modulus of the first derivative of the dipole moment with respect to Q_p:

$$A_p \propto \left| \frac{\partial \mu}{\partial Q_p} \right|^2 = \sum_i \bar{Z}^2_{p,i} \tag{9}$$

The Berry phase scheme for the derivative of the dipole moment

The theoretical framework of the Berry Phase scheme implemented in Crystal is reported in detail in Ref. 8. We report here the main equations for purposes of comparison with the other methods. The difference in electronic polarization between a deformed geometry (1) and the equilibrium geometry (0), according to the Berry phase theory[6,7] is:

$$\Delta \mathbf{P}_{el} = -\frac{i}{(2\pi)^3} \int d\mathbf{k} \left[\left\langle \Phi^{(1)}(\mathbf{k}) \right| \nabla_{\mathbf{k}} \Phi^{(1)}(\mathbf{k}) \right\rangle - \left\langle \Phi^{(0)}(\mathbf{k}) \left| \nabla_{\mathbf{k}} \Phi^{(0)}(\mathbf{k}) \right\rangle \right] \tag{10}$$

where

$$\left|\Phi^{(\lambda)}(\mathbf{k})\right\rangle = \frac{1}{\sqrt{n!}}\left|u_1^{(\lambda)}(\mathbf{k})\,\bar{u}_1^{(\lambda)}(\mathbf{k})\ldots u_{n/2}^{(\lambda)}(\mathbf{k})\,\bar{u}_{n/2}^{(\lambda)}(\mathbf{k})\right| \tag{11}$$

and $u_i(\bar{u}_i)$ is the periodic part of the i-th HF occupied spin $\alpha(\beta)$ crystalline orbital in the Bloch form:

$$\psi_i^{(\lambda)}(\mathbf{r},\mathbf{k}) = \mathrm{e}^{i\mathbf{k}\cdot\mathbf{r}} u_i^{(\lambda)}(\mathbf{r},\mathbf{k}) \quad . \tag{12}$$

The reader must take care not to confuse the $u_1^{(\lambda)}$, that represent occupied crystalline orbitals here, with the $u_{\alpha,j}$ of eq. 2 and 3, that represent atomic displacements.
In Eqs.(10)-(12) $\lambda = 1$ and $\lambda = 0$ refer to the deformed and equilibrium geometry respectively.

The way the integral in Eq. 10 is implemented is explained in detail in Ref. 8 and in the Supplementary Material section, where we report other technical details.

Computational Implementations of the periodic Foster-Boys localization

The orbital localization usually considered in the context of molecular electronic structure calculations can be extended to periodic systems through the use of generalized Wannier functions (WFs). Given a particular reference WF (assigned to a reference cell), $\omega(\mathbf{r})$, the family of its translational images forms an orthonormal set, i.e.

$$\int d\mathbf{r}\; \omega(\mathbf{r})^* \omega(\mathbf{r}-\mathbf{R}_\mathbf{g}) = \langle\omega|\omega^\mathbf{g}\rangle = \delta_{0g_1}\delta_{0g_2}\delta_{0g_3}, \tag{13}$$

where $\mathbf{R}_\mathbf{g} = g_1\mathbf{a}_1 + g_2\mathbf{a}_2 + g_3\mathbf{a}_3$ denotes a lattice vector, $\mathbf{g} \equiv (g_1, g_2, g_3)$ and integration is over the whole coordinate space. Each reference WF $\{\omega_i(\mathbf{r})\}$, in turn, may be written in terms of an AO basis set as[10]

$$\omega_i(\mathbf{r}) = \sum_{\mu=1}^{M}\sum_{\mathbf{g}} c_{\mu i}^{\mathbf{g}} \varphi_\mu(\mathbf{r}-\mathbf{s}_\mu-\mathbf{R}_\mathbf{g}). \tag{14}$$

where $\mathbf{s}_\mu$ is the position of the atom in the reference cell. The sum over $\mathbf{g}$ on the rhs of eq. 14 is convergent by virtue of the exponential decay of WFs[27] and the AOs. In numerical implementations this sum is truncated so as to consider just those terms whose coefficients $c_{\mu i}^{\mathbf{g}}$ are smaller in absolute value than a given threshold.

As previously proposed,[11,28] the periodic extension of the Foster-Boys localization requires a minimization of the spatial spread functional,

$$\Omega(\{\omega_i\}) = \sum_i \langle\omega_i|\mathbf{r}^2|\omega_i\rangle - \langle\omega_i|\mathbf{r}|\omega_i\rangle^2, \tag{15}$$

where the sum on the rhs is over all reference WFs in the orthonormal set $\{\omega_i(\mathbf{r})\}$ and the functional $\Omega(\{\omega_i\})$ depends upon the specific choice of such a set. This yields a straightforward extension of the stationary condition[11] adopted in the molecular case

$$\langle\omega_i|\mathbf{r}|\omega_j^{\mathbf{g}}\rangle \cdot (\langle\omega_i|\mathbf{r}|\omega_i\rangle - \langle\omega_j|\mathbf{r}|\omega_j\rangle - \mathbf{R}_g) = 0. \tag{16}$$

The localized WFs (LWFs) form a new orthonormal set that satisfies the previous conditions through an orthogonal transformation of the original set of reference WFs, together with their translational images, according to

$$\omega_i'(\mathbf{r}) = \sum_{q=0}^{\infty} \sum_{\mathbf{g}}^{|\mathbf{R}_{\mathbf{g}}|=R_q} \sum_j O_{ji}^{\mathbf{g}}\, \omega_j(\mathbf{r} - \mathbf{R}_{\mathbf{g}}). \tag{17}$$

Here the sum over q includes all ordered lattice vectors with the modulus, $R_0 = 0$, $R_q < R_{q+1}$; the sum over $\mathbf{g}$ includes those lattice vectors whose modulus is R_q; and the sum over j includes all original reference WFs. The matrix $O_{ji}^{\mathbf{g}}$ is translationally invariant. Given the decay of the WFs: $\lim_{q\to\infty} |O_{ij}^{\mathbf{g}}| = 0$, the first sum can be truncated after a maximum value, $q_{\max}$, in numerical applications. In most optimization methods the determination of $O_{ji}^{\mathbf{g}}$ depends upon calculating all the matrix elements in eq. 16 (see more below).

Although there are algorithms[11] that allow one to obtain a suitable set $\{\omega_i'(\mathbf{r})\}$, two

practical problems arise that make their application difficult:

1. In the original Foster-Boys formulation the localization process can start with any subset of canonical orbitals since the canonical and localized orbitals both exhibit the same exponential decay. This is not the case for periodic systems in which the canonical orbitals are Bloch functions (BF) that necessarily lack this property owing to their translational invariance.[29] Therefore, the application of the previous scheme requires a suitable guess for the WFs to initiate the optimization procedure.

2. The calculation of the dipole matrix elements in eq. 16 that are used in constructing the orthogonal transformation matrix $O_{ij}^{\mathbf{g}}$ is computationally demanding. Even if truncation criteria can be adopted to limit the set of numerically relevant components there remain a large number depending strongly on the degree of localization of the WFs. The less localized the set of reference WFs, the larger will be that number.

In the CRYSTAL code a localization scheme called Wannier-Boys (WB)[11,30] has been implemented to overcome these drawbacks. It is a mixed scheme that consists of an initial step in which the canonical orbitals are transformed into a set of WFs and, then, localized through a restricted Boys process in which just a few dipole moment matrix elements are explicitly computed. It has been shown that the iterative (see later) application of these steps provides LWFs that may be used to start a full Foster-Boys periodic localization through eq. 16 and/or 17 . The latter are sufficiently well-localized for the accurate computation of the WF centroids and the IR intensities.

More details on the localization scheme are presented in the Supplementary Information.

The CPHF/KS method

The BP and WF methods outlined in the two preceding sections both involve a numerical differentiation (in reciprocal space in the first case – see Eq. 10; in real space in the second case associated with displacement of the WF centroid) for evaluating the Born charges Z^*

of eq. 4. The analytical evaluation of such quantities is not straightforward because the unit cell dipole moment in periodic systems depends on an arbitrary choice of the unit cell.[5,31] One solution to this fundamental concern has now been provided within the Modern Theory of Polarization (MTP)[6,31,32] and the Vector Potential Approach (VPA).[22,33]

In order to appreciate that solution we recall that the expression for the dipolar interaction between a molecular electron and a uniform electric field E is given by

$$\hat{Z}(\mathbf{r}) = \mathcal{E} \cdot \mathbf{r} \quad . \tag{18}$$

When applied to an infinite periodic system, however, this expression is unbound and breaks translational invariance.

This problem has been tackled by several authors.[21,22,33–38] Their common approach relies on an alternative formulation of the electronic interaction operator which, in the Bloch basis, is diagonal with respect to the reciprocal space $\mathbf{k}$ vector. Provided the system has a non-zero bandgap, this operator may be written as:

$$\hat{\Omega}(\mathbf{k}) = \imath\mathcal{E} \cdot e^{\imath\mathbf{k}\cdot\mathbf{r}} \nabla_k e^{-\imath\mathbf{k}\cdot\mathbf{r}} \quad . \tag{19}$$

Then, the wavefunction and electric field response properties can be obtained through a periodic Coupled-pertubed Hartree-Fock (CPHF) or Kohn-Sham (CPKS) approach. Such a CPHF/CPKS treatment has recently been developed[39,40] and implemented,[23,24] by some of the present authors, in the Crystal program.[41] The recent addition of the DIIS accelerator[42] has further improved the efficiency and stability of the procedure. A brief but detailed description of the key elements of the CPHF/KS method, as implemented in CRYSTAL, is reported in the last section of the Supplementary Information. Here we recall only the final formula actually implemented in the code.

Our goal is to obtain a computable expression for the Born charge tensor elements Eq.4. This is obtained by differentiating the total energy expression with respect to a generic field

direction $\mathcal{E}_j$ (in the zero field limit) and with respect to the displacement of atom α along direction i:

$$\left.\frac{\partial}{\partial \mathcal{E}_j}\frac{\partial E}{\partial u_{\alpha i}}\right|_{\mathcal{E}=0} = \frac{1}{n_{\mathbf{k}}}\sum_{\mathbf{k}} \mathrm{Tr}\left[\mathfrak{F}^{(u_{\alpha i})}(\mathbf{k})D^{(\mathcal{E}_j)}(\mathbf{k}) + \left(\mathfrak{F}^{(u_{\alpha i})}\right)^{(\mathcal{E}_j)}(\mathbf{k})D^{(0)}(\mathbf{k}) - S^{(u_{\alpha i})}(\mathbf{k})D_W^{(\mathcal{E}_j)}(\mathbf{k})\right] + Z_A\delta_{ij} \tag{20}$$

in which the notation $\mathfrak{F}^{(u_{\alpha i})}$ means that the derivative of the Fock matrix is taken with the density matrix held fixed at its equilibrium geometry value. Although the basis functions that determine Fock matrix do depend upon geometry it is worth recalling that they do not depend on the external field. In eq. 20 Tr signifies the trace and the field-perturbed eigenvalue-weighted density matrix

$$\begin{aligned} D_W^{(\mathcal{E}_j)}(\mathbf{k}) &= \left(\alpha^{[\mathcal{E}_j]}(\mathbf{k})\,\epsilon^{[0]}(\mathbf{k})\,n\,\alpha^{[0]\dagger}(\mathbf{k})\right. \\ &+ \alpha^{[0]}(\mathbf{k})\,\epsilon^{[\mathcal{E}_j]}(\mathbf{k})\,n\,\alpha^{[0]\dagger}(\mathbf{k}) \\ &+ \left.\alpha^{[0]}(\mathbf{k})\,\epsilon^{[0]}(\mathbf{k})\,n\,\alpha^{[\mathcal{E}_j]\dagger}(\mathbf{k})\right) \end{aligned} \tag{21}$$

has been introduced. Here n is the diagonal occupation number matrix with eigenvalues equal to two for occupied orbitals and zero for virtual orbitals.

Evaluation of eq. 21 involves the occupied diagonal block of $\Omega_j(\mathbf{k})$ through $\epsilon^{(\mathcal{E}_j)}(\mathbf{k})$. The occupied diagonal block of $\Omega_j(\mathbf{k})$, in turn, is partially undetermined (see refs. 37, 43, 44). This aspect is related to the arbitrary phase in the BP scheme or, alternatively, to the translational invariance of the Wannier Functions in the WF scheme.

We have demonstrated[25,26] that, fortunately, the *occ–occ* block of $\Omega_j(\mathbf{k})$ that appears in D_W is canceled by contributions from the other terms in eq. 20 so that, in the end, the infrared intensity is completely determined. It should be noted that the expression for the IR intensity, eq. 20, does not contain any terms involving the perturbed wavefunction due to atomic displacements. As a consequence, the computational steps required to solve eq. 20 are: i) self-consistent solution of the CPHF/KS equations along the three Cartesian

directions ii) evaluation of integral (monoelectronic, bielectronic, overlap) gradients at the equilibrium geometry and iii) assembly of all the quantities.
The extension from CPHF to CPKS requires the derivative of the exchange-correlation energy with respect to the atomic displacement and electric field. For this purpose the analytical expression for the energy gradient is exploited. Its derivative with respect to the electric field depends on the solution of the CPHF/KS equations (for more details, see Ref. 25).

Results

The main interest in this paper on the calculation of IR intensities using the CRYSTAL code is to (i) test the numerical stability of the three different approaches with respect to the tunable computational parameters, (ii) assess under which conditions the three schemes provide comparable results and (iii) compare the computational cost of the three approaches as currently implemented. This assessment includes the effort required to generate the Hessian – needed for vibrational frequencies and normal modes – through mixed analytical/numerical second derivatives.

Our discussion deals solely with internal comparisons. Comparison with other codes has been possible for molecular systems, for which the same functional and basis set can be used. In that case the agreement is excellent. With regard to periodic systems, this comparison is much more difficult, due to many differences between computer codes (plane-waves *vs* Gaussian type functions, *all electron vs* pseudopotential, pure DFT *vs hybrid* functionals). No comparison with experiment is made, since that would imply a thorough analysis of the experimental error bars and a careful examination of the effect of basis set and functional, which is beyond the scope of this work.

Assessing the computational parameters

In order to check the effect of the main computational parameters and thresholds on the accuracy of the IR intensities evaluated with the three different methods, we have chosen two prototypical systems. One is the quartz crystal in its α structure, which has 9 atoms per unit cell and belongs to the space group $P3_221$ with 6 point group symmetry operators and 12 IR active modes. Due to symmetry, only 5 displaced geometries, instead of 3x9=27 are needed for the construction of the Hessian matrix, if eq. 2 is used (this number should be doubled if eq. 3 is adopted).

The other prototypical system is pyrope, which has 80 atoms per unit cell and belongs to the space group $Ia\bar{3}d$ with 48 point group symmetry operators and 17 IR active modes. In this case only 8 displaced geometries are required for building the Hessian matrix.

For the first system, the PBEsol[45] functional was adopted; the basis set is a 6-31G* contraction for O[46] and a 6-631G* contraction for Si[47]. As usual, the first shell is of s type. It is followed by sp type shells and, finally, the asterisk stands for a polarization d shell. There are a total of 138 contracted Atomic Orbitals (AOs) in the unit cell.

For pyrope, we used the B3LYP[48,49] functional; the basis set is the same as in references 14 and 50: an 8-511G* contraction for Mg, 8-611G* for Al, 8-6311G* for Si and 8-411G* for O. This leads to a total of 1488 contracted AOs in the unit cell, about 10 times larger than in α-quartz.

The reason for using different functionals for the two cases examined here is that PBEsol and B3LYP probe different parts of the code in the integral part (the exchange-correlation contribution to the Fock matrix is evaluated numerically in pure DFT; the exchange integrals are evaluated analytically for the fraction of the Hartree-Fock exchange in B3LYP). The integral part is called recursively in the CPHF scheme. Errors might then appear in one case and not in the other. The very similar quality of the results will confirm that both implementations are correct.

The slightly different basis set adopted for the O and Si atoms, that appear in both investi-

gated systems, is related to the different ionic nature of the two systems (α-quartz is more covalent).

The three different schemes for the calculation of the IR intensity are controlled by a substantial number of parameters. Default values, which may be considered safe with respect to the numerical accuracy of the results, have been available for some time now. Here we will limit most of the analysis to the two that are, by far, the most important and delicate. They are also the most frequently varied when the accuracy of the calculated property values needs to be checked.

The first of these parameters is the shrinking factor IS for the commensurate net[51] that defines the number of **k** points at which the Fock operator is diagonalized (this number is IS^3, when there is no point group symmetry). All the subsequent calculations are based on the eigenvalues and eigenvectors obtained at this set of points. The effect of the number of **k** points on the IR intensities can, in principle, be very different for the three schemes. In the BP method IS determines the 'step size' for the finite differences in eq. S.4 (see Supplementary Information) as well as the number of terms in the discretized eq. S.3. In the WF approach, this parameter has an impact on the size of the direct space cyclic cluster for which the set of WFs is defined. This connection is implicit in eq. S.8 , i.e. for reasonable results the number of sampling points in the **k** space must be comparable to the number of direct space cells used for the description of the WF.

We note that the CP approach benefits from relying fully on analytical derivatives. Hence, it is less dependent on the density of the Brillouin-zone sampling. The threshold for the convergence of the self-consistent first order coupled-perturbed cycles are set to very tight values (10^{-4} a.u. in the value of the polarizability), which is generally achieved in 5-6 iterative cycles,[42] and is not a sensitive parameter.

The second key set of computational parameters are the thresholds controlling the truncation (thus, accuracy) of the infinite series of bielectronic integrals contributing to the Fock operator. The effect of these parameters propagates along the entire chain of calculation:

SCF eigenvalues and eigenvectors→ total energy → equilibrium geometry → construction of the Hessian → calculation of the IR intensities. The tolerances T_i, i=1 to 5, control the truncation of the Coulomb ($i = 1$ and 2) and exchange ($i = 3$,4 and 5) series. A full definition of these parameters can be found in ref. 52. Roughly speaking, they correspond to terminating the series when the overlaps between s-type gaussians used to simulate integrals, or penetration between charge distributions, are smaller than 10^{-x} where x is the value of the parameter. Here we will employ just a single parameter that determines the value of all the T_i. Thus, in the following $T_x = j$ must be understood as j, j, j, j, 2j for the five parameters. In all calculations presented here convergence on the total energy during the SCF cycle has been set to 10^{-8} Hartree for the geometry optimization, and 10^{-10} Hartree for the wavenumber calculation.

α-quartz: intensities and wavenumbers

The 12 IR active modes of α-quartz belong to the E and A_2 irreducible representations. of the C_{3v} point group. Both the normal modes and the corresponding wavenumbers are determined by diagonalizing the Hessian. The wavenumbers are shown in Table 1 as a function of IS and Tx, respectively. In the first part of the table the statistical indices show that the effect of the IS parameter on the wavenumbers is extremely small. At IS=3 the maximum difference with respect to IS=9 is just 0.04 cm^{-1}. In the second part of the table, $|\overline{\Delta}|$ and $|\Delta_{max}|$ (the mean absolute difference and the maximum difference with respect to the reference case, Tx = 8) are both in the range 0.5-1.5 cm^{-1}, for Tx=7 and Tx=9, and increase to 2.5 and 4.7 for the looser tolerance Tx=6. So we can conclude that the wavenumbers are already well converged when relatively small parameter values, such as IS=3 and Tx=7, are used.

The effect of the computational parameters on the normal modes – via the Hessian – can be viewed through the behavior of the IR intensities, which is shown in Table 2, as a function of the IS parameter, and in Table 3, as a function of the Tx parameter. In Table 2 the

indices $|\overline{\delta}|$ and $|\delta_{max}|$ measure the difference of the IR intensities between the three methods at fixed IS. At variance with respect to wavenumbers, the intensities span several orders of magnitude. Hence, it is important to judge the differences on a percentage rather than an absolute basis. In spite of some relatively large differences (particularly for WF) in going from IS=3 to IS=6, the three methods provide intensities that coincide to within .04 percent from IS=6 on.

We turn now to the effect of the Tx parameter on the IR intensities. As in the case of the wavenumbers, the IR intensities are more sensitive to Tx than to IS over the range of parameters considered (see Table 3). However, the differences between the three methods for fixed Tx (see $|\overline{\delta}|$ and $|\delta_{max}|$) remain extremely small (1-2 km/mol compared to, say, the average intensity $\overline{I}$, which is of the order of 600 km/mol). In addition, the differences between the three schemes as a function of Tx are very limited; Δ_{max} is always less than 10 km/mol for Tx=7, 8 and 9. The largest difference is for mode 10, whose intensity is about 3560 km/mol, which means that the percentage difference is smaller than 3%.

As a final remark on α-quartz, we comment on three other computational parameters that could, in principle, significantly influence the accuracy of the calculation of the IR intensities. These parameters have been tested and found not to affect the results in the present case, hence the results are not shown. The first is the grid for the numerical integration of the exchange-correlation contribution to the Fock operator (the XLGRID and XXLGRID options in CRYSTAL17, see ref. 52, were compared). The second is the number of points used for the numerical construction of the Hessian matrix (equations 2 and 3 were compared), and the third is the step used in these equations (0.003 and 0.01 Å were compared). In the three cases $|\overline{\delta}|$ and $|\delta_{max}|$ essentially coincide with the ones shown in Tables 2 and 3.

Pyrope: intensities and wavenumbers

Pyrope is one of the most important members of the garnet family. IR intensities and full spectra of garnets have already been studied with CRYSTAL, adopting the BP and WF

approaches, in a number of works.[14,50] Here Tables 4 - 6 report the same quantities that were shown in Tables 1 - 3 for α-quartz. The trends are very similar, so that the analysis can be more brief.

The convergence of the wavenumbers with increasing IS and Tx (Table 4) is very fast; for the lowest IS and Tx values (2 and 7, respectively) well converged results are obtained (the largest value for $|\Delta_{max}|$ is less than 2 cm^{-1} for IS=2 and smaller than 0.2 cm^{-1} in all other cases).

Let us consider now the IR intensities. Whereas in α-quartz the range of intensities is from 1 (mode 1 of the list) to 3600 (mode 10 of the list) km/mol, for pyrope the minimum intensity is as small as 0.01 (mode 4) and the maximum is as large as 14000 km/mol (mode 15). Similarly, $\overline{I}$ is about five times larger for pyrope; roughly, 3600 compared to 640 Km/mol for α-quartz. The quantity $|\delta_{max}|$, which is a measure of the maximum difference between methods, is associated with the very intense peak 15 in pyrope. Its value is, nonetheless, smaller than 2% of $\overline{I}$ for IS larger than 3 in Table 5 and for Tx larger than 7 in Table 6. We conclude that the numerical stability of all three methods remains roughly the same when increasing the size and complexity of the system.

The reader may note that in table 5 the WF column for IS=2 contains zeros. That is because the formation of WFs fails due to an insufficient number of k points, and then of direct space cells, included in the process (see the discussion just after eq. S.9 in Supplementary Information). From IS=3 on, however, the localization converges. So, whereas all quantities are quite reasonably converged at IS=2 for the BP and CPHF/KS methods, the WF approach requires a slightly denser reciprocal space net.

Discussion and Conclusions

The three schemes implemented in the CRYSTAL code[41,52] for the evaluation of the IR intensities of crystalline solids, differ greatly in the specific numerical steps that are involved, such

as: truncation of infinite summations, discrete sampling of the Brillouin zone, analytical or numerical derivatives and thresholds for the convergence of self consistent procedures.

Here we comment on the relative costs of the three schemes, with respect to one another and with respect to the fraction of the total cost associated with the construction and diagonalization of the Hessian matrix (let us call it TH, Time for Hessian). All timings reported are total CPU times as obtained on 8 Intel Xeon CPU E5-2690 v4@2.60GHz nodes, 14 cores per node, for a total 112 cores. The wall–clock time is roughly obtained dividing the reported total times by this number. For pyrope, Table 4 shows that TH ranges from 200 (IS=2, Tx=7) to 466 hours (IS=3, Tx=9) depending upon the tolerances and shrinking factor. The total time for IR intensities (Tables 5 and 6) For the BP method the total time ranges from about 6 to 81 hours. So the cost is always a fraction of TH (from 3% to 25% at the two extremes) and is more dependent on the number of k points than on integral tolerances. The total time for the WF scheme is higher: from 109 to 342 hours, so that in the more severe conditions the calculation of IR intensity costs about the same as TH. For the CP method the corresponding numbers are, roughly speaking, similar to the WF ones (from 113 to 276 hours).

These timing figures do not represent the ideal relative efficiencies since part of the difference between them is due to history.

The core part of the Berry Phase approach was the first to be implemented (1997)[8] and is simpler than the other two: it does not rely on iterative procedures, involves only little linear algebra, and does not require Fock matrix builds. Therefore, this algorithm was ported to a massively parallel implementation of CRYSTAL already in the 2014 release and applied to the study of large-scale models, up to an order of magnitude larger than pyrope. Examples of such models are ibuprofen adsorbed in MCM-41 mesoporous silica[53] (a system that features 12054 atomic orbitals in the unit cell) and the B defect (a vacancy surrounded by 4 N atoms) in diamond[54] – the largest supercell studied contains 1000 atoms, with T_d point symmetry and 8991 AOs in the basis set. The WF and CP schemes utilize much more complex al-

gorithms and are, at least in the present implementation, considerably more demanding in terms of memory and time. On the other hand the CP approach, in particular, is more open to greater efficiency through further algorithmic developments, such as analytical second derivatives (i.e. the Hessian). It is also worth noticing that, if Raman intensities are to be computed, the CP scheme remains as the only choice.[55,56] In that case, the Born charges are obtained almost as a by–product of the Raman tensor.

In other words, we have here an evidence of the general rule that evolution of software is always slower than that of the hardware (speed of the CPU, parallel architecture).

Acknowledgements

The present manuscript took long time in the making, almost 10 years. In this timespan, two people have contributed to the implementation of the methods here presented, and to the writing of this work, who are no longer with us and cannot be listed as co-authors even if they would deserve it.

Alessio Meyer, a PhD student at that time, successfully worked in porting the Berry Phase scheme for polarization by Dall'Olio et al.[8] to the IR intensity calculation. Alessio left us soon after that, in december 2009, due to heart attack.

Claudio Zicovich Wilson was the developer of the Wannier Function scheme in CRYSTAL and contributed to the writing of the relative theoretical section. Claudio Zicovich Wilson suddenly passed away due to a heart attack in 2016.

All the present authors take this occasion to remember Claudio, a very good friend and an excellent scientist, and for recognizing his major contribution to this manuscript and, more generally, to the development of the CRYSTAL code, and to remember Alessio, a good-hearted person and a hard worker.

References

(1) Prencipe, M. Quantum Mechanics in Earth Sciences: a One-Century-Old Story. *Rendiconti Lincei. Scienze Fisiche e Naturali* **2018**, 1–21.

(2) Chavan, S.; Vitillo, J. G.; Gianolio, D.; Zavorotynska, O.; Civalleri, B.; Jakobsen, S.; Nilsen, M. H.; Valenzano, L.; Lamberti, C.; Lillerud, K. P. et al. H 2 Storage in Isostructural UiO-67 and UiO-66 MOFs. *Physical Chemistry Chemical Physics* **2012**, *14*, 1614–1626.

(3) Galimberti, D.; Milani, A.; Maschio, L.; Castiglioni, C. Intermolecular Modulation of IR Intensities in the Solid State. The Role of Weak Interactions in Polyethylene Crystal: A Computational DFT Study. *The Journal of Chemical Physics* **2016**, *145*, 144901.

(4) Ruggiero, M. T.; Sibik, J.; Orlando, R.; Zeitler, J. A.; Korter, T. M. Measuring the Elasticity of Poly-l-Proline Helices with Terahertz Spectroscopy. *Angewandte Chemie International Edition* **2016**, *55*, 6877–6881.

(5) Resta, R. Manifestations of Berry's Phase in Molecules and Condensed Matter. *J. Phys. Condens. Mat.* **2000**, *12*, R107–R143.

(6) Resta, R. Macroscopic Polarization in Crystalline Dielectrics: The Geometric Phase Approach. *Rev. Mod. Phys.* **1994**, *66*, 809.

(7) King-Smith, R.; Vanderbilt, D. First-Principles Investigation of Ferroelectricity in Perovskite Compounds. *Phys. Rev. B* **1994**, *49*, 5828.

(8) Dall'Olio, S.; Dovesi, R.; Resta, R. Spontaneous Polarization as a Berry Phase of the Hartree-Fock Wavefunction: The Case of $KNbO_3$. *Phys. Rev. B* **1997**, *56*, 10105–10114.

(9) Noel, Y.; Zicovich-Wilson, C. M.; Civalleri, B.; D'arco, P.; Dovesi, R. Polarization Properties of ZnO and BeO: An ab initio Study Through the Berry Phase and Wannier Functions Approaches. *Phys. Rev. B* **2002**, *65*, 014111.

(10) Zicovich-Wilson, C. M.; Dovesi, R.; Saunders, V. R. A General Method to Obtain Well-Localized Wannier Functions for Composite Energy Bands in Linear Combination of Atomic Orbital Periodic Calculations. *J. Chem. Phys.* **2001**, *115*, 9708–9719.

(11) Zicovich-Wilson, C. M.; Dovesi, R. In *Beyond Standard Quantum Chemistry: Applications from Gas to Condensed Phases*; Hernandez-Lamoneda, R., Ed.; Transworld Research Network, Trivandrum, Kerala, India, 2007; Vol. 125; pp 140–169.

(12) Zicovich-Wilson, C. M.; Bert, A.; Roetti, C.; Dovesi, R.; Saunders, V. R. Characterization of the Electronic Structure of Crystalline Compounds Through their Localized Wannier Functions. *J. Chem. Phys.* **2002**, *116*, 1120–1127.

(13) Baranek, P.; Zicovich-Wilson, C. M.; Roetti, C.; Orlando, R.; Dovesi, R. Well-Localized Crystalline Orbitals Obtained from Bloch Functions: The Case of $KNbO_3$. *Phys. Rev. B* **2001**, *64*, 125102.

(14) Zicovich-Wilson, C. M.; Torres, F. J.; Pascale, F.; Valenzano, L.; Orlando, R.; Dovesi, R. Ab initio Simulation of the IR Spectra of Pyrope, Grossular, and Andradite. *J. Comp. Chem.* **2008**, *29*, 2268–2278.

(15) Pisani, C.; Busso, M.; Capecchi, G.; Casassa, S.; Dovesi, R.; Maschio, L.; Zicovich-Wilson, C.; Schütz, M. Local-MP2 Electron Correlation Method for Nonconducting Crystals. *J. Chem. Phys.* **2005**, *122*, 094113.

(16) Maschio, L.; Usvyat, D.; Manby, F. R.; Casassa, S.; Pisani, C.; Schütz, M. Fast Local-MP2 Method with Density-Fitting for Crystals. I. Theory and Algorithms. *Phys. Rev. B* **2007**, *76*, 075101.

(17) Pisani, C.; Maschio, L.; Casassa, S.; Halo, M.; Schütz, M.; Usvyat, D. Periodic Local MP2 Method for the Study of Electronic Correlation in Crystals: Theory and Preliminary Applications. *J. Comp. Chem.* **2008**, *29*, 2113–2124.

(18) Hurst, G. J. B.; Dupuis, M.; Clementi, E. Ab initio Analytic Polarizability, First and Second Hyperpolarizabilities of Large Conjugated Organic Molecules: Applications to Polyenes C_4H_6 to $C_{22}H_{24}$. *J. Chem. Phys.* **1988**, *89*, 385.

(19) Karna, S. P.; Dupuis, M. Frequency Dependent Nonlinear Optical Properties of Molecules: Formulation and Implementation in the HONDO Program. *J. Comp. Chem.* **1991**, *12*, 487.

(20) Blount, E. I. *Solid State Physics*; H. Ehrenreich, F. Seitz and D. Turnbull: Academic, New York, 1962; Vol. 13; p 305.

(21) Otto, P. Calculation of the Polarizability and Hyperpolarizabilities of Periodic Quasi-One-Dimensional Systems. *Phys. Rev. B* **1992**, *45*, 10876.

(22) Kirtman, B.; Gu, F. L.; Bishop, D. M. Extension of the Genkin and Mednis Treatment for Dynamic Polarizabilities and Hyperpolarizabilities of Infinite Periodic Systems. I. Coupled Perturbed Hartree–Fock theory. *J. Chem. Phys.* **2000**, *113*, 1294.

(23) Ferrero, M.; Rérat, M.; Orlando, R.; Dovesi, R. The Calculation of Static Polarizabilities of 1-3D Periodic Compounds. The Implementation in the CRYSTAL Code. *J. Comp. Chem.* **2008**, *29*, 1450–1459.

(24) Ferrero, M.; Rérat, M.; Orlando, R.; Dovesi, R. Coupled Perturbed Hartree-Fock for Periodic Systems: The Role of Symmetry and Related Computational Aspects. *J. Chem. Phys.* **2008**, *128*, 014110.

(25) Maschio, L.; Kirtman, B.; Orlando, R.; Rérat, M. Ab initio Analytical Infrared Intensities for Periodic Systems Through a Coupled Perturbed Hartree-Fock/Kohn-Sham Method. *J. Chem. Phys.* **2012**, *137*, 204113.

(26) Maschio, L.; Kirtman, B.; Rérat, M.; Orlando, R.; Dovesi, R. Comment on "Ab initio Analytical Infrared Intensities for Periodic Systems Through a Coupled Perturbed

Hartree-Fock/Kohn-Sham Method" [J. Chem. Phys. 137, 204113 (2012)]. *J. Chem. Phys.* **2013**, *139*, 167101.

(27) Kohn, W. Analytic Properties of Bloch Waves and Wannier Functions. *Phys. Rev.* **1959**, *115*, 809–821.

(28) Marzari, N.; Vanderbilt, D. Maximally Localized Generalized Wannier Functions for Composite Energy Bands. *Phys. Rev. B* **1997**, *56*, 12847–12865.

(29) Zicovich-Wilson, C. M.; Erba, A. A Fundamental Connection Between Symmetry and Spatial Localization Properties of Basis Sets. *Theor. Chem. Acc.* **2010**, *126*, 165.

(30) Zicovich-Wilson, C. M.; Dovesi, R. A General Method to Obtain Well-Localized Wannier Functions for Composite Energy Bands in Linear Combination of Atomic Orbital Periodic Calculations. *J. Chem. Phys.* **2001**, *115*, 9708–9719.

(31) King-Smith, R.; Vanderbilt, D. First-Principles Investigation of Ferroelectricity in Perovskite Compounds. *Phys. Rev. B* **1993**, *47*, 1651.

(32) Resta, R. Quantum-Mechanical Position Operator in Extended Systems. *Phys. Rev. Lett.* **1998**, *80*, 1800–1803.

(33) Gu, F. L.; Bishop, D. M.; Kirtman, B. Crystal Orbital Calculation of Coupled Hartree–Fock Dynamic (Hyper)Polarizabilities for Prototype Π-Conjugated Polymers. *J. Chem. Phys.* **2001**, *115*, 10548–10556.

(34) Champagne, B.; Fripiat, J. G.; André, J. From Uncoupled to Coupled Hartree–Fock Polarizabilities of Infinite Polymeric Chains. Pariser–Parr–Pople Applications to the Polyacetylene Chains. *J. Chem. Phys.* **1992**, *96*, 8330–8337.

(35) Otto, P.; Gu, F. L.; Ladik, J. Calculation of ab initio Dynamic Hyperpolarizabilities of Polymers. *J. Chem. Phys.* **1999**, *110*, 2717–2726.

(36) Kudin, K. N.; Scuseria, G. An Efficient Finite Field Approach for Calculating Static Electric Polarizabilities of Periodic Systems. *J. Chem. Phys.* **2000**, *113*, 7779.

(37) Bishop, D. M.; Gu, F. L.; Kirtman, B. Coupled-Perturbed Hartree–Fock Theory for Infinite Periodic Systems: Calculation of Static Electric Properties of $(LiH)_n$, $(FH)_n$, $(H_2O)_n$, $(–CNH–)_n$, and $(–CH=CH–)_n$. *J. Chem. Phys.* **2001**, *114*, 7633–7643.

(38) Otto, P.; Martinez, A.; Czaja, A.; Ladik, J. Electron Correlation Corrected Static Polarizabilities of Polymers with Linear and Cyclic Conjugated Elementary Cells. *J. Chem. Phys.* **2002**, *117*, 1908–1914.

(39) Ferrero, M.; Rérat, M.; Kirtman, B.; Dovesi, R. Calculation of First and Second Static Hyperpolarizabilities of One- to Three-Dimensional Periodic Compounds. Implementation in the CRYSTAL Code. *J. Chem. Phys.* **2008**, *129*, 244110.

(40) Kirtman, B.; Maschio, L.; Rérat, M.; Springborg, M. *Frontiers of Quantum Chemistry*; Springer, 2018; pp 87–115.

(41) Dovesi, R.; Erba, A.; Orlando, R.; Zicovich-Wilson, C. M.; Civalleri, B.; Maschio, L.; Rérat, M.; Casassa, S.; Baima, J.; Salustro, S. et al. Quantum-mechanical Condensed Matter Simulations with CRYSTAL. *Wiley Interdiscip. Rev. Comput. Mol. Sci.* **2018**, e1360.

(42) Maschio, L. Direct Inversion of the Iterative Subspace (DIIS) Convergence Accelerator for Crystalline Solids Employing Gaussian Basis Sets. *Theo. Chem. Acc.* **2018**, *137*, 60.

(43) Kudin, K. N.; Car, R.; Resta, R. Berry Phase Approach to Longitudinal Dipole Moments of Infinite Chains in Electronic-Structure Methods with Local Basis Sets. *J. Chem. Phys.* **2007**, *126*, 234101.

(44) Izmaylov, A.; Scuseria, G. Analytical Infrared Intensities for Periodic Systems with Local Basis Sets. *Phys. Rev. B* **2008**, *77*, 165131.

(45) Perdew, J. P.; Ruzsinszky, A.; Csonka, G. I.; Vydrov, O. A.; Scuseria, G. E.; Constantin, L. A.; Zhou, X.; Burke, K. Restoring the Density-Gradient Expansion for Exchange in Solids and Surfaces. *Phys. Rev. Lett.* **2008**, *100*, 136406.

(46) Gatti, C.; Saunders, V. R.; Roetti, C. Crystal Field Effects on the Topological Properties of the Electron Density in Molecular Crystals: The Case of Urea. *J. Chem. Phys.* **1994**, *101*, 10686–10696.

(47) Francl, M. M.; Pietro, W. J.; Hehre, W. J.; Binkley, J. S.; Gordon, M. S.; DeFrees, D. J.; Pople, J. A. Self-Consistent Molecular Orbital Methods. XXIII. A Polarization-Type Basis Set for Second-Row Elements. *J. Chem. Phys.* **1982**, *77*, 3654–3665.

(48) Becke, A. D. Density-Functional Thermochemistry. III. The Role of Exact Exchange. *J. Chem. Phys.* **1993**, *98*, 5648–5652.

(49) Lee, C.; Yang, W.; Parr, R. Development of the Colle-Salvetti Correlation-Energy Formula Into a Functional of the Electron Density. *Phys. Rev. B* **1988**, *37*, 785–789.

(50) Pascale, F.; Wilson, C. M. Z.; Orlando, R.; Roetti, C.; Ugliengo, P.; Dovesi, R. Vibration Frequencies of $Mg_3Al_2Si_3O_{12}$ pyrope. An ab initio Study with the CRYSTAL Code. *J. Phys. Chem. B* **2005**, *109*, 6146–6152.

(51) Monkhorst, H. J.; Pack, J. D. Special Points for Brillouin-Zone Integrations. *Phys. Rev. B* **1976**, *13*, 5188.

(52) Dovesi, R.; Saunders, V. R.; Roetti, C.; Orlando, R.; Zicovich-Wilson, C. M.; Pascale, F.; Civalleri, B.; Doll, K.; Harrison, N. M.; Bush, I. J. et al. CRYSTAL17 User's Manual. 2017.

(53) Delle Piane, M.; Corno, M.; Pedone, A.; Dovesi, R.; Ugliengo, P. Large-Scale B3LYP Simulations of Ibuprofen Adsorbed in MCM-41 Mesoporous Silica as Drug Delivery System. *J. Phys. Chem. C* **2014**, *118*, 26737–26749.

(54) Salustro, S.; Ferrari, A. M.; Gentile, F. S.; Desmarais, J. K.; Rérat, M.; Dovesi, R. Characterization of the B-center Defect in Diamond Through the Vibrational Spectrum. A Quantum Mechanical Approach. *J. Phys. Chem. A* **2018**, *122*, 594–600.

(55) Maschio, L.; Kirtman, B.; Rérat, M.; Orlando, R.; Dovesi, R. Ab initio Analytical Raman Intensities for Periodic Systems Through a Coupled Perturbed Hartree-Fock/Kohn-Sham Method in an Atomic Orbital Basis. I. Theory. *J. Chem. Phys.* **2013**, *139*, 164101.

(56) Maschio, L.; Kirtman, B.; Rérat, M.; Orlando, R.; Dovesi, R. Ab initio Analytical Raman Intensities for Periodic Systems Through a Coupled Perturbed Hartree-Fock/Kohn-Sham Method in an Atomic Orbital Basis. II. Validation and Comparison with Experiments. *J. Chem. Phys.* **2013**, *139*, 164102.

Table 1: Influence of the shrinking factor IS (at Tx=8) and of Tx (at IS=9) on the wavenumbers ν (cm^{-1}) of the twelve IR active modes of α-quartz, calculated with PBEsol[45]. The symmetry of the mode is indicated. $|\overline{\Delta}|$ is the mean absolute difference with respect to the reference case (IS=9). $|\Delta_{max}|$ is the maximum absolute error with respect to the same reference.

	IS				Tx			
Mode #	3	6	9	12	6	7	8	9
1 E	122.30	122.28	122.28	122.28	126.39	123.72	122.28	120.96
2 E	243.20	243.20	243.19	243.20	245.04	243.41	243.20	242.52
3 A_2	313.91	313.88	313.88	313.88	312.94	313.81	313.88	313.91
4 E	355.49	355.47	355.47	355.47	355.85	355.35	355.47	355.30
5 E	413.26	413.27	413.27	413.27	416.42	413.72	413.27	412.40
6 A_2	464.03	464.03	464.03	464.03	467.39	464.58	464.03	463.03
7 E	680.42	680.40	680.40	680.40	682.56	680.98	680.40	680.12
8 A_2	753.26	753.26	753.26	753.26	752.66	753.45	753.26	753.40
9 E	785.32	785.27	785.27	785.27	786.92	785.98	785.27	784.86
10 E	1023.89	1023.92	1023.92	1023.92	1020.06	1023.73	1023.92	1025.29
11 A_2	1036.28	1036.30	1036.31	1036.31	1033.32	1036.03	1036.31	1037.52
12 E	1106.05	1106.07	1106.07	1106.07	1101.34	1105.53	1106.07	1107.61
$\|\overline{\Delta}\|$	0.06	0.00	-	0.00	2.48	0.45	-	0.75
$\|\Delta_{max}\|$	0.04	0.00	-	0.00	4.73	1.44	-	1.55

IS / Mode #	3			6			9			12		
	BP	WF	CP	BP	WF	CP	BP	WF	CP	BP	WF	CP
1	1	0	1	1	1	1	1	1	1	1	1	1
2	32	32	30	30	30	29	30	30	29	30	30	29
3	212	217	205	208	206	206	207	206	206	207	206	206
4	295	250	285	290	288	288	289	288	288	288	288	288
5	715	705	700	703	699	700	701	699	700	700	699	700
6	355	350	350	352	351	350	351	351	350	351	351	350
7	95	157	91	92	91	91	91	91	91	91	91	91
8	259	243	252	255	254	254	254	254	254	254	254	254
9	285	258	281	279	276	276	277	276	276	277	276	276
10	3562	3668	3560	3564	3563	3564	3564	3563	3564	3564	3563	3564
11	1866	1855	1877	1874	1877	1877	1875	1877	1877	1876	1877	1877
12	88	33	87	86	86	86	86	86	86	86	86	86
$\overline{I}$	647	647	643	644	643	643	644	643	644	644	643	643
$\lvert\overline{\delta}\rvert$	-	29	6	-	1	2	-	1	1	-	0	0
$\lvert\delta_{max}\rvert$	-	107	15	-	4	3	-	2	2	-	1	2
$\lvert\overline{\Delta}\rvert$	5	27	2	1	1	1	-	1	1	0	1	1
$\lvert\Delta_{max}\rvert$	14	105	15	2	2	3	-	2	2	1	2	2

Table 2: Influence of the shrinking factor (IS) on the intensity of the twelve IR active modes of α-quartz, calculated with PBEsol[45] and using Tx= 8 for the truncation of the bielectronic integrals. Intensities are given in km/mol. $\overline{I}$ is the mean intensity, $|\overline{\delta}|$ is the mean absolute difference evaluated with respect to the BP column for each IS value (that is, with reference to columns 1, 4, 7, 10). $|\delta_{max}|$ is the maximum value of the absolute difference. $|\overline{\Delta}|$ and $|\Delta_{max}|$ have the same meaning, but this time the reference for the full set of columns is BP with IS=9.

Mode # \ Tx	6			7			8			9		
	BP	WF	CP	BP	WF	CP	BP	WF	CP	BP	WF	CP
1	1	1	1	1	1	1	1	1	1	1	1	1
2	32	31	32	30	30	29	30	30	30	30	30	29
3	204	203	203	208	207	207	207	206	206	208	207	207
4	291	290	293	289	288	289	289	288	288	289	289	289
5	694	693	694	702	700	703	701	699	700	702	700	701
6	343	342	341	349	348	348	351	351	350	354	353	353
7	100	100	100	93	92	92	91	91	91	89	89	89
8	274	274	272	257	257	256	254	254	254	248	248	248
9	276	274	274	276	275	275	277	276	276	278	276	276
10	3529	3528	3532	3556	3556	3557	3564	3563	3564	3574	3573	3574
11	1859	1860	1859	1872	1873	1875	1875	1877	1877	1881	1883	1884
12	92	91	92	88	88	88	86	86	86	83	83	83
$\overline{I}$	641	641	641	643	643	643	644	643	644	645	644	644
$\lvert\overline{\delta}\rvert$	-	1	1	-	1	1	-	1	1	-	1	1
$\lvert\delta_{max}\rvert$	-	2	3	-	2	3	-	2	2	-	2	2
$\lvert\overline{\Delta}\rvert$	9	9	9	2	20	2	-	1	1	3	3	3
$\lvert\Delta_{max}\rvert$	35	36	3	7	8	3	-	2	2	10	9	2

Table 3: Influence of the tolerances Tx controlling the truncation of the infinite Coulomb and exchange series on the intensity of the twelve IR active modes of α-quartz, calculated with PBEsol[45] and using IS=9. Intensities are given in km/mol. Symbols and units as in previous tables.

Table 4: Influence of the shrinking factor IS (Tx=7) and of the Tx tolerance (IS=3) controlling the truncation of the Coulomb and exchange infinite summations on the wavenumbers ν (cm^{-1}) of the 17 IR active modes of pyrope, calculated with B3LYP. TCP is the total CPU time, in hours, required by the calculation of the Hessian matrix. Four nodes of 28 cores each, for a total of 112 cores, have been used. Symbols and units as in previous tables.

	IS				Tx		
Mode #	2	3	4	6	7	8	9
1	113.64	115.21	113.67	115.35	113.66	113.64	113.65
2	137.06	137.88	137.06	137.93	137.04	137.06	137.04
3	184.92	185.62	184.92	185.59	184.89	184.92	184.89
4	213.00	213.67	212.99	213.60	212.97	213.00	212.96
5	258.63	258.88	258.64	258.82	258.64	258.63	258.64
6	332.65	332.65	332.65	332.63	332.64	332.65	332.66
7	345.82	346.20	345.83	346.28	345.82	345.82	345.83
8	379.57	380.16	379.60	380.30	379.57	379.57	379.59
9	420.80	421.01	420.87	420.96	420.81	420.80	420.85
10	456.57	456.90	456.62	456.89	456.55	456.57	456.61
11	480.32	481.31	480.35	481.42	480.33	480.32	480.33
12	530.44	531.08	530.48	531.12	530.44	530.44	530.48
13	580.21	580.63	580.23	580.76	580.18	580.21	580.23
14	672.79	673.09	672.76	672.96	672.73	672.79	672.76
15	864.83	864.86	864.82	864.82	864.83	864.83	864.83
16	895.93	895.99	895.95	895.95	895.95	895.93	895.95
17	970.31	970.37	970.28	970.29	970.25	970.31	970.28
$\lvert\overline{\Delta}\rvert$	0.49	0.07	0.01		0.02	0.02	-
$\lvert\Delta_{max}\rvert$	1.71	0.14	0.03		0.06	0.05	-
TCP	200	247	285	312	247	338	466

Mode #	IS=2			IS=3			IS=4			IS=6		
	BP	WF	CP	BP	WF	CP	BP	WF	CP	BP	WF	CP
1	3101	-	3101	3101	3098	3100	3098	3099	3102	3100	3101	3102
2	33	-	31	32	32	31	32	32	31	32	32	32
3	3309	-	3299	3303	3299	3298	3300	3299	3297	3303	3300	3294
4	0	-	0	0	0	0	0	0	0	0	0	0
5	641	-	647	646	646	649	646	647	647	645	646	647
6	6409	-	6369	6384	6372	6368	6374	6372	6372	6383	6372	6370
7	45	-	43	45	45	43	44	44	44	44	44	44
8	3456	-	3452	3457	3449	3458	3450	3450	3446	3453	3448	3451
9	1370	-	1367	1367	1359	1370	1368	1367	1370	1368	1367	1368
10	13696	-	13672	13689	13681	13664	13676	13671	13669	13672	13673	13667
11	859	-	843	852	847	842	846	847	841	851	846	842
12	793	-	798	794	795	798	798	798	800	798	799	799
13	1423	-	1402	1412	1407	1402	1408	1405	1403	1408	1404	1404
14	3	-	3	3	3	3	3	3	3	3	3	3
15	14151	-	14054	14100	14056	14043	14068	14055	14050	14082	14055	14040
16	5672	-	5657	5668	5670	5673	5666	5672	5663	5668	5668	5669
17	5833	-	5787	5802	5788	5780	5793	5785	5786	5798	5787	5789
$\overline{I}$	3576	-	3560	3568	3562	3560	3565	3561	3560	3562	3561	3560
$\lvert\overline{\delta}\rvert$	-	-	17	-	6	10	-	4	6	-	2	4
$\lvert\delta_{max}\rvert$	-	-	96	-	44	57	-	26	41	-	13	18
$\lvert\overline{\Delta}\rvert$	14.46	-	3	6	3	5	3	2	4	-	2	4
$\lvert\Delta_{max}\rvert$	82.91	-	13	32	12	25	14	12	27	-	13	18
TCP	6	109	113	27	166	155	47	227	174	81	342	202

Table 5: Influence of the shrinking factor (IS) on the intensity of the 17 IR active modes of pyrope, calculated with B3LYP and using Tx= 7 for the truncation of the bielectronic integrals. Intensities in km/mol. TCP is the total CPU time, in hours, required by the calculation of the IR intensity. Four nodes of 28 cores each have been used. Symbols and units as in Table 2.

Mode # \ Tx	7			8			9		
	BP	WF	CP	BP	WF	CP	BP	WF	CP
1	3101	3098	3100	3050	3049	3048	3042	3047	3042
2	32	32	31	36	35	35	38	39	38
3	3303	3299	3298	3309	3304	3302	3311	3302	3308
4	0	0	0	0	0	0	0	0	0
5	646	646	649	654	656	658	655	656	657
6	6384	6372	6368	6429	6419	6416	6421	6396	6402
7	45	45	43	51	50	51	49	48	49
8	3457	3449	3458	3485	3480	3483	3483	3474	3465
9	1367	1360	1370	1291	1285	1283	1326	1327	1325
10	13689	13681	13664	13733	13732	13725	13684	13711	13697
11	852	847	842	879	869	869	917	897	904
12	794	795	798	746	750	751	735	738	739
13	1412	1407	1402	1425	1415	1416	1441	1430	1432
14	3	3	3	2	2	2	3	2	2
15	14050	14056	14043	14112	14052	14047	14103	14046	14050
16	5668	5670	5673	5683	5688	5692	5681	5691	5682
17	5802	5788	5780	5794	5775	5773	5798	5781	5774
$\overline{I}$	3568	3562	3560	3569	3562	3562	3570	3564	3563
$\lvert\overline{\delta}\rvert$	-	7	10	-	8	10	-	12	10
$\lvert\delta_{max}\rvert$	-	44	57	-	60	65	-	57	53
$\lvert\overline{\Delta}\rvert$	22	26	29	11	17	17	-	12	9
$\lvert\Delta_{max}\rvert$	66	70	76	50	50	55	-	57	53
TCP	27	166	155	24	199	199	29	222	276

Table 6: Influence of the tolerances Tx that control the truncation of the infinite Coulomb and exchange series on the intensity of the 17 IR active modes of pyrope, calculated with B3LYP and using IS=3. Intensities are given in km/mol. TCP is the total CPU time, in hours, required by the calculation of the IR intensity. Four nodes of 28 cores each have been used. Symbols and units as in Table 2.

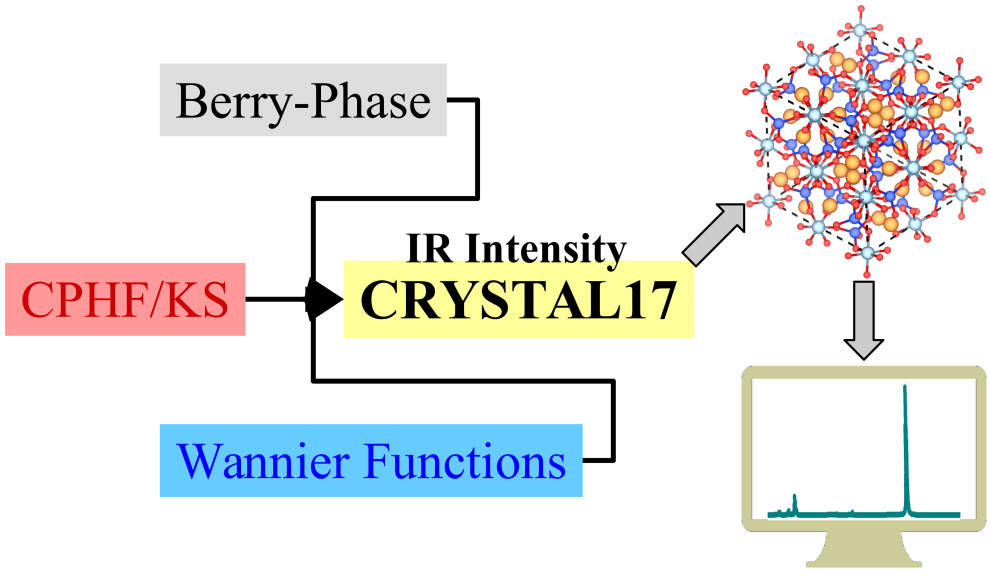
Berry-Phase
IR Intensity
CPHF/KS
CRYSTAL17
Wannier Functions

TOC Graphic